Original Article

Journal of Intelligent Material Systems and Structures

Journal of Intelligent Material Systems and Structures
2016, Vol. 27(2) 208–220

DOI: 10.1177/1045389X14563869
jim.sagepub.com
SAGE

Shear thickening fluid–based energy-free damper: Design and dynamic characteristics

Hong Zhou[1], Lixun Yan[2], Wanquan Jiang[3], Shouhu Xuan[1] and Xinglong Gong[1]

Abstract

Shear thickening fluid exhibits a tremendous ability to dissipate energy under an un-expected attack by presenting an abrupt increase in viscosity. In this work, a novel prototype shear thickening fluid damper was fabricated and its dynamic characteristics were experimentally investigated. By varying the rheological properties of the shear thickening fluids, the final shear thickening fluid dampers with different mechanical characteristics were obtained. The mechanism was qualitatively analyzed, and it was observed that the output force of shear thickening fluid damper sharply increased as soon as an external stimulus was imposed. The maximum output force of this shear thickening fluid damper can reach to as high as 2.7 kN, which was several orders of magnitude higher than the conventional shear thickening fluid damper. The model composed of an equivalent linear stiffness term, and a power-law viscous damping term was proposed and it agreed well with the nonlinear performance of shear thickening fluid damper.

Keywords

shear thickening fluid, energy dissipation, shear thickening fluid–based damper

Introduction

Impact resistance and vibration attenuation are very important in industrial and military applications; thus, various methods were developed to reduce the energy during impact and vibration. Among them, viscous liquid dampers were proved to be very effective, and the common viscous damper was filled with Newtonian fluid which possessed a constant viscosity. The force generated in damper depends on the viscosity of fluid and the relative velocity between piston and damper shell, in which the last point cannot be changed once the damper was fabricated. Therefore, the smart materials whose rheological properties can be controlled by an external field have attracted increasing interests to construct high-performance intelligent dampers. During the past decades, electrorheological (ER) fluid and magnetorheological (MR) fluid have been widely studied and applied to intelligent dampers in seismic protectors for high-rise buildings and automotive suspensions (Dyke et al., 1996; Jolly et al., 1999; Zong et al., 2013), due to the rheological properties of the ER/MR fluids which can be changed when subjected to external electric and magnetic fields, respectively. The previous research indicated that the ER/MR fluid–based devices such as shock absorbers, clutches, brakes, actuators, artificial joints, and isolations show better performances than other conventional devices (Bica et al., 2013; Kim et al., 2002; Lee and Choi, 2000; Li and Du, 2003; Wereley et al., 1998). However, an external power source is needed in these devices, and this disadvantage increases the weight and complexity of devices. To sort this out, novel smart fluid–based dampers with energy-free characteristics are pressingly required due to their special advantages in the practical application.

Shear thickening fluid (STF) is a highly concentrated colloidal suspension that consists of monodisperse particles suspended in carry fluids. When the STF suspension is subjected to a sudden stimulus such as shear rate

[1]CAS Key Laboratory of Mechanical Behavior and Design of Materials, Department of Modern Mechanics, University of Science and Technology of China, Hefei, People's Republic of China
[2]Department of Precision Machinery & Instrumentation, University of Science and Technology of China, Hefei, People's Republic of China
[3]Department of Chemistry, University of Science and Technology of China, Hefei, People's Republic of China

Corresponding author:
Xinglong Gong, CAS Key Laboratory of Mechanical Behavior and Design of Materials, Department of Modern Mechanics, University of Science and Technology of China, Hefei 230027, China.
Email: gongxl@ustc.edu.cn

or shear stress, its rheological property changed from a flowable behavior into a rigid behavior. Beyond a critical shear rate, STF shows a steep increase in viscosity, transforming from a liquid to solid-like state (Barnes, 1989; Fall et al., 2012). This transformation is instantaneous and reversible; thus, the viscosity of STF recovers quickly to the initial value when external shear rate or shear stress is removed (Bender and Wagner, 1996; Jiang et al., 2010). Over the last few decades, the preparation method and the influencing factors on its rheological properties under steady and oscillatory shear flow were intensively investigated (Brown et al., 2010; Jiang et al., 2010; Maranzano and Wagner, 2001; Ye et al., 2013). A lot of efforts have been taken on its mechanism via rheo-optical experiments, neutron scattering, and numerical simulation (Boersma et al., 1995; Cheng et al., 2011; Foss and Brady, 2000; Lee and Wagner, 2006; Maranzano and Wagner, 2002). The obtained order–disorder mechanism depicts that an ordered laminar flow at low shear rates disrupts into a disordered viscous flow at high shear rates due to particle interaction (Hoffman, 1998), while the hydrocluster mechanism demonstrates that clusters of particles are formed in the ST behavior because hydrodynamic lubrication forces are higher than repulsive forces at critical shear rate and the viscosity recovers due to the breakups of clusters (Barnes, 1989). Moreover, discontinuous shear thickening (DST) phenomenon is also investigated to analyze the ST behavior, in which the dilation frustrated by boundary condition is considered to be the key point for the discontinuous increase in viscosity by several orders of magnitude (Brown and Jaeger, 2014).

STFs have a great potential for energy dissipation and absorption because their viscosity can experience an abrupt rise in critical shear rate. Therefore, they can be applied in both energy-free protecting and damping devices, such as speed controller, body armor, passive damped system, and blast wave protection (Dawson et al., 2009; Fischer et al., 2010; Iyer et al., 2013; Laun et al., 1991; Lee et al., 2003; Srivastava et al., 2012). STF-based dampers are novel intelligent apparatus that the damping can increase abruptly, along with an increase in viscosity of STF under vibration or impact, and that it will decrease quickly when the vibration or impact is removed. Helber et al. (1990) developed an STF-based mount and discussed its performance of vibration attenuation. Zhang et al. (2008) reported a prototype STF damper in flow mode and studied its dynamic properties under various loading conditions. These typical studies proved the practical possibility of an STF damper. However, the detailed analysis of the vibration attenuation mechanism and affecting factors is still lacking. Moreover, the STFs' properties directly determine the characteristics of the STF damper. Unfortunately, no work has been done to definitely demonstrate their inter-relationship. To our knowledge, the previously reported STF dampers only possessed a very small output force which largely confined their practical applications. Therefore, a high-performance STF damper with intense ST behavior is pressingly needed.

In this work, STF samples composed of colloid particles dispersed in ethylene glycol (EG) were fabricated. By changing the particle volume fractions, STF samples with different rheological properties were obtained. Then, a prototype STF damper was conducted and its dynamic properties under various loading conditions were tested. The effects of particle concentration of STF samples and geometry parameters of STF damper were experimentally investigated. The mechanisms of different phenomena of STF dampers were also analyzed. Based on the analysis of the energy dissipation of the STF damper, a potential model that can well describe the nonlinear properties of STF damper at shear-thickened state was proposed.

Design of STF damper

The common viscous damper is usually divided into two types with respect to the piston rod. A damper composed of a single-ended piston rod has less size in the axial direction than a double-ended piston damper, but an attached compensation structure is needed to adjust the internal volume of the single-ended piston damper which varies with the forward and backward movements of the piston. Thus, the structure of a double-ended piston damper is much simpler.

In addition, according to the viscous fluid flow, the damper can be divided into flow and shear modes. In the two modes, the force is generated when the viscous fluid flows through the orifices in the piston head and the annular gap between the cylinder and piston head, respectively. The energy dissipation and absorption of an STF-based damper depend on the dramatic increase in the viscosity of STF. It may be easily jammed in the orifices with a high viscosity. Therefore, the STF-based damper in a shear mode is more tractable.

In this work, an STF damper was designed with a double-ended piston rod and an annular gap. Its schematic and prototype are shown in Figure 1. The cylinder, piston, and guide sleeves are made of Q235 steel, stainless steel, and aluminum, respectively. The guide sleeves are placed at both ends of the cylinder to ensure the straight reciprocating motion of piston rod. In order to enclose STF in cylinder chamber, nitrile rubber seal rings are attached to the piston rod. When the piston moves forward or backward, the STF is pushed through the annular gap. With an increase in piston velocity, the viscosity of STF abruptly increases and even transforms to the solid-like state. Therefore, the output force of STF-based damper increases quickly. By varying the viscosity of STF and the geometry of the annular gap (the diameter and length of the piston

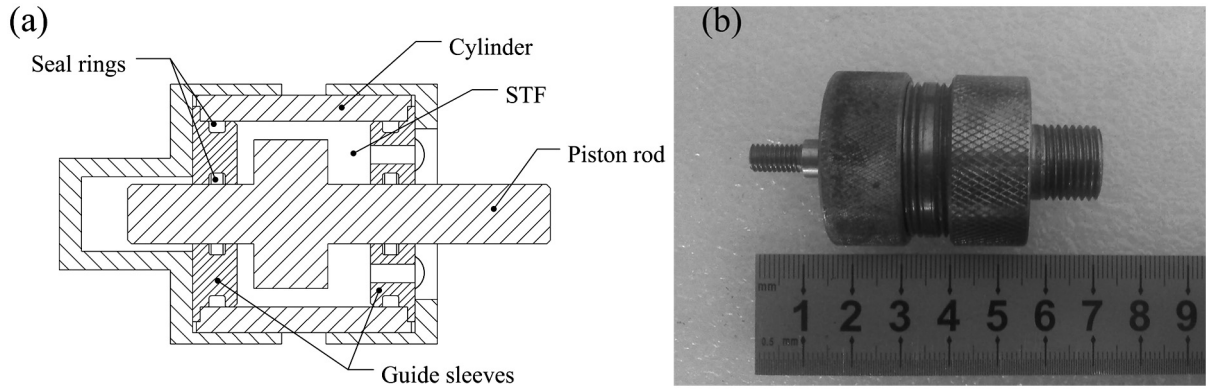

Figure 1. The (a) schematic and (b) prototype of the STF damper.

Table 1. Parameters of dampers.

Number	Piston length (mm)	Piston diameter (mm)	Annular gap (mm)
Damper-1	8	20	2.5
Damper-2	8	22	1.5
Damper-3	10	22	1.5

head), the output force of STF damper can be altered. In this work, three pistons with different geometries were prepared. The maximum stroke of STF damper is 8 mm, and the parameters of dampers used in the experiment are shown in Table 1.

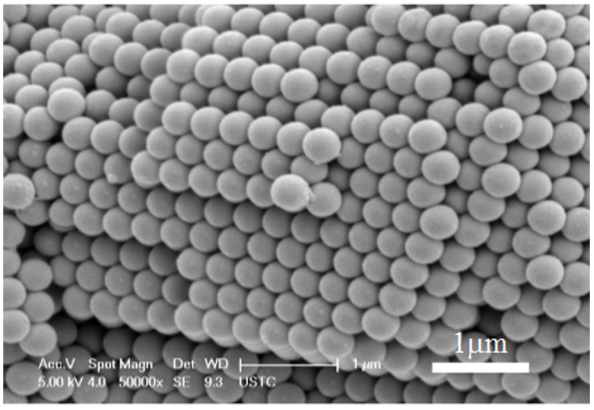

Figure 2. SEM image of PSt–EA copolymer particles.

Experiment details

Preparation of STF samples

All reagents used in this work were purchased from Sinopharm Chemical Reagent Co. Ltd (Shanghai, China). The polystyrene (PSt)–ethyl acrylate (EA) particles were prepared by styrene (St), EA, and acrylic acid (AA) via emulsion polymerization. St was purified with NaOH before being used. The polymerization was conducted in a three-necked flask, which was in a 70°C water bath, and fixed with a mechanical stirrer, a reflux condenser, and a nitrogen inlet. Potassium persulfate (KPS) was added as initiator. After 6 h in water bath, the resultants were collected by centrifugation after the polymerization. The PSt–EA particles were cleaned by distilled water three times and dried in a vacuum oven at 50°C. The microstructure of PSt–EA particles was investigated by scanning electron microscope (SEM; Sirion 200, FEI Co., Holland). As shown in Figure 2, the particles were monodisperse spheres with an average diameter of 390 nm. The STF samples were obtained by dispersing the PSt–EA particles into EG with milling in a ball crusher for 24 h. Then, the samples were handled by ultrasonic processing for 1 h to remove air bubbles. Three kinds of STF samples with particle volume fraction of 60%, 65%, and 67% were prepared.

Rheological testing

A cone-plate rheometer (MCR 301; Anton-Paar Company, Germany) was used to measure the rheological properties of samples under oscillation loading conditions. The diameter of the cone-plate is 25 mm and the cone angle is 0.2°. The surface roughness of the cone-plate is less than 0.5 μm. The experiments were performed with a gap size of 0.05 mm by dynamic amplitude sweep in which angular frequency was fixed at 20 rad s^{-1}. The shear strain amplitude changed from 1% to 2000%, corresponding to a shear rate from 0.2 to 400 s^{-1}.

Fabrication and dynamic testing of STF damper

After incorporating the STF into the damper, the final STF damper was obtained. They were defined as Damper-*x*-*y*%STF, in which *x* represents the geometry

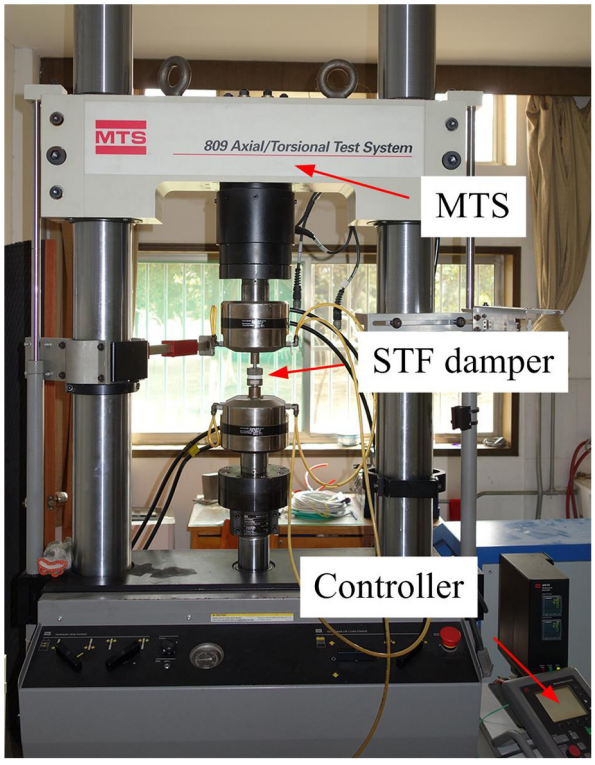

Figure 3. Schematic picture of the experiment setup.

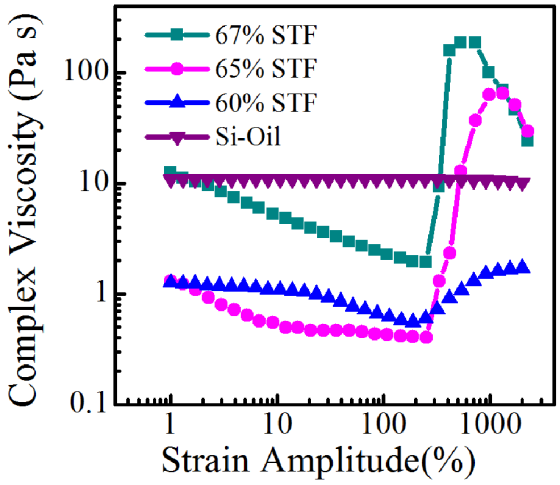

Figure 4. Complex viscosity versus shear strain amplitude for STFs and silicon oil.

of the damper listed in Table 1 and y the particle volume fraction of STF. The MTS809 TestStar Material Testing System was used to test the dynamic performance of the STF damper. As shown in Figure 3, the STF damper was vertically located in the testing heads. Both ends of it were fixed by two V block fixtures. The excitation signal was driven by the hydraulic system in the bottom of MTS, and it was measured by the linear variable differential transformer (LVDT). When the under-head of MTS moved upward and downward by a command signal generated from the control computer, the force and displacement signals were obtained from the sensors in the testing head and fed to the control computer. All the signals were collected in the control computer by a data sampling system for further operation. In each test, the excitation signal was a sinusoidal-varying displacement of fixed frequency and amplitude. The excited frequencies were varied from 0.1 to 5 Hz, and the displacement amplitudes were 1, 2, and 3 mm, respectively. All the tests were repeated for at least 20 cycles, and the data were obtained from the stabilized hysteresis loops.

Results and discussion

Rheological properties of STF

Three kinds of STF samples with different particle volume fractions of 60%, 65%, and 67% were measured under oscillation loading conditions. As a comparison, pure methyl silicon oil (Si-Oil) with a constant viscosity of 12,500 cSt was also used to construct an Si-Oil damper. The complex viscosity, η, was a function of shear strain amplitude for STF and Si-Oil. Figure 4 shows the typical shear strain amplitude–dependent viscosities of the STFs and Si-Oil solutions. As a traditional fluid, the viscosity of the Si-Oil was kept as a constant over the test range. However, the STFs exhibited a special manner, and the ST effect was highly influenced by the volume fraction. By increasing shear strain amplitude, the viscosities of 65 and 67 v/v% STF first decreased and then increased abruptly. Due to the low concentration, an increase in viscosity of the 60 v/v% STF was relatively small. In this work, ST behavior appeared once the volume fraction increased beyond 60 v/v%. The increase in viscosity was relatively mild for low concentrated STF due to the hydroclustering in microstructure transition (referred to as "continuous shear thickening" (CST)). With an increase in the particle concentration beyond 65 v/v%, the viscosity jumped discontinuously by orders of magnitude (referred to as DST). Obviously, such a large increase in viscosity is not responded to the lubrication forces in hydroclustering but can be ascribed to the dilation with boundary confinement. The maximum viscosity of 67 v/v% STF is 180 Pa s, which is much higher than that of 65 v/v% STF (60 Pa s) and 60 v/v% STF (2 Pa s). Since severe shear thickening leads to a fluid–solid phase transition, a slipping will happen at the interfaces between STF and the cone-plate during the testing. In this case, the viscosities of 65 v/v% STF and 67 v/v% STF declined quickly at high shear strain amplitude after they reached the maximum value. The viscosity of Si-Oil sample kept a constant value of 10 Pa s and showed a

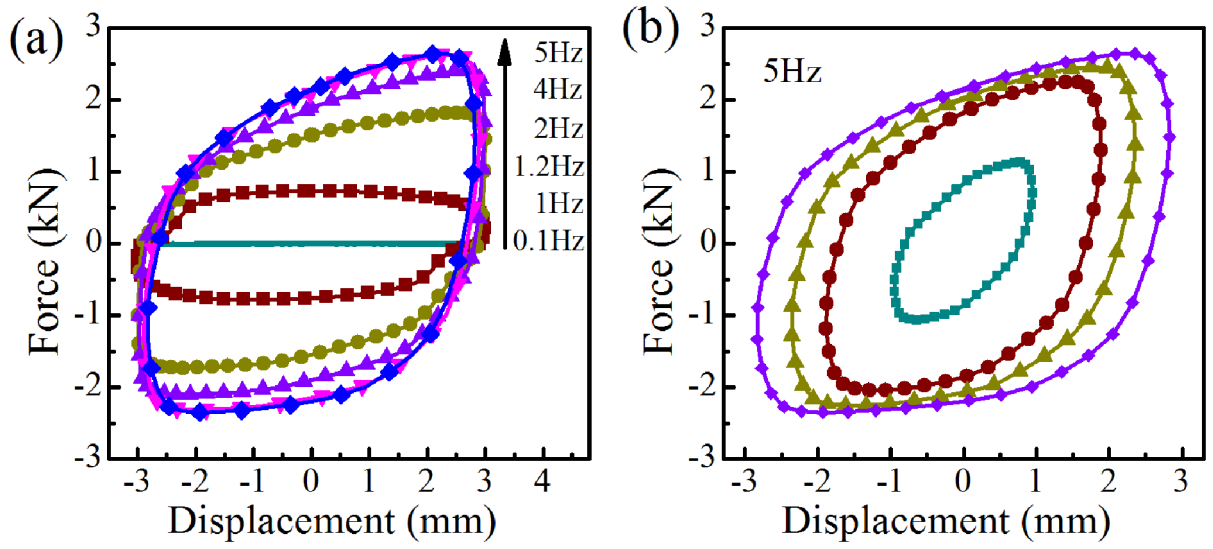

Figure 5. Dynamic properties of damper-2-67%STF at various frequencies and amplitudes: (a) A = 3 mm and (b) f = 5 Hz.

perfect Newtonian fluid behavior over the test range. The initial viscosities of 67 v/v% STF and Si-Oil were both 10 Pa s, larger than that of 65 v/v% STF and 60 v/v% STF (1 Pa s). It can be deduced that the viscous force generated from Si-Oil will be larger than that from 60 v/v% STF, but lower than that from 65 v/v% STF at high shear strain amplitude. Furthermore, we can also find that the critical shear strain amplitude for 65 v/v% STF and 67 v/v% STF are about 300%, corresponding to the shear rate of 60 s^{-1}, as the onset of shear thickening behavior.

Properties of STF damper

The dynamic properties of damper-2-67%STF were measured under sinusoidal-varying displacement stimuli, and the force versus displacement at different frequencies and amplitudes was obtained (Figure 5). Typical hysteresis loops of STF damper at certain amplitude and frequency are shown in Figure 5(a) and 5(b), respectively. The force of STF damper was very sensitive to excited frequency and amplitude, which indicated that the dynamic property of STF damper was rate-dependent. As shown in Figure 5(a), when the excited frequency was lower than 1 Hz, ST behavior did not appear in the damper and the force was much smaller. Beyond a certain frequency (or critical frequency), the viscosity of STF increased suddenly and the output force of STF damper reached a maximum value of 2.7 kN, which was dozens of times larger than that obtained below critical frequency. However, the frequency showed little influence on the output force when it was larger than 4 Hz, which demonstrated that the force reached saturation at high frequency. Moreover, when the amplitude was 1 mm, the

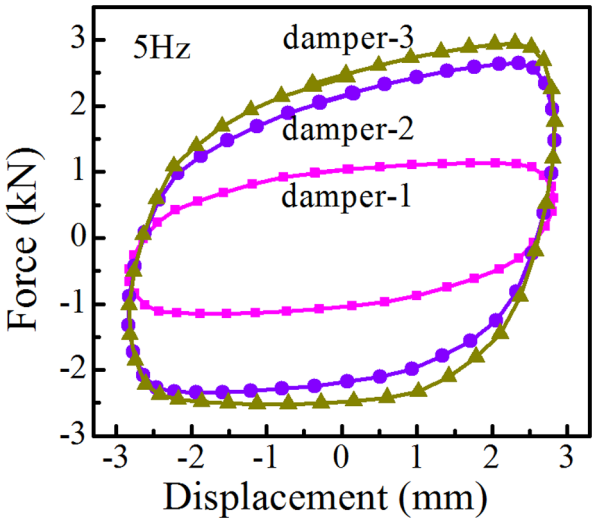

Figure 6. Force versus displacement of STF dampers with different pistons (67 v/v% STF).

hysteresis loop of force was an ellipse, which indicated the damper presented a linear viscoelastic behavior (Figure 5(b)). As the amplitude increased, the force increased and also reached a stable value. The shape of the loops departed from an ellipse, which demonstrated an obvious amplitude-dependent nonlinear viscoelastic behavior. The maximum output force of STF damper was 2.7 kN, which was several orders of magnitude higher than the conventional STF damper and proved a more widely practical possibility for engineering application (Zhang et al., 2008).

In addition, the hysteresis loops distorted at the ends of stroke when the frequency just exceeded the critical

value (such as the loop at frequency of 1 Hz in Figure 5(a)). The load direction of the hysteresis loops was clockwise and the force kept a relatively large value when the piston approached the ends of stroke. It is ascribed to the unrecovered solidification of STF. Because of the sinusoidal-varying excited displacement, the piston velocity reached maximum when the displacement was 0. At the critical frequency, the maximum piston velocity exceeded the critical value, and this led to the shear thickening. When the piston compressed to the ends of stroke, STF recovered due to the decrease in the piston velocity. However, the compressing force did not decrease rapidly until the piston stopped at the ends of stroke on account of the remains of solidification. Finally, the piston changed moving direction, and the force decreased to 0 and then increased with piston velocity again.

Effects of geometry on the STF damper

In order to investigate the effect of geometry on the STF damper, dampers with various pistons were also prepared and tested (Figure 6). The geometry parameters are shown in Table 1. It was observed that the force increased dramatically from 1 to 2.7 kN when the annular gap between the cylinder and the piston head decreased from 2.5 to 1.5 mm. However, when the piston length increased from 8 to 10 mm, a small increase in the output force was obtained. Interestingly, similar phenomena were also found at high frequency and amplitude. Here, the ratio of viscous force to total force decreased due to the solidification of STF; thus, the force increased slowly with the piston length. The narrowing of annular gap led to a large increment in output force, but the piston length had little influence on the STF damper.

Effects of STF rheological property on the STF damper

Output force. The rheological property of the STF had a high influence on the damper's characteristics. Figure 7 presents the force versus displacement behavior of damper-2-65%STF at various frequencies and amplitudes. It can be seen that the force was kept at almost a constant value at low frequency. As soon as the testing frequency exceeded a certain value, the force mildly increased. Interestingly, with an increase in the amplitude, the critical frequency decreased from 3 to 2 Hz. In comparison with damper-2-67%STF (Figure 5(a)), the maximum viscosity of 65 v/v% STF reduced from 180 to 60 Pa s; thus, the critical frequency increased from 1 to 3 Hz and the maximum output force reduced from 2.7 to 0.3 kN at a frequency of 5 Hz. The continuously increased force was different from the discontinuously increased force in damper-2-67%STF beyond the critical frequency, which resulted from the difference between the CST behavior of 65 v/v% STF and DST behavior of 67 v/v% STF. Moreover, the shape of hysteresis loop of damper-2-65%STF looked more like an ellipse, which showed the linear viscoelastic characteristics. Based on the above analysis, we can conclude that the damper's characteristics are highly influenced by the rheological property of STF.

Here, the ST behavior plays a key role on the high performance of the STF damper. Replacing the STF by pure Si-Oil, a traditional damper-2-SiOil was obtained. Figure 8 gives the curves of force–displacement at various frequencies and amplitudes for damper-2-SiOil. The Si-Oil sample is a Newtonian fluid and has a constant viscosity of 10 Pa s, which is higher than that of 60 v/v% STF (1 Pa s). For damper-2-60%STF, a constant damper force of 60 N was observed and the loops

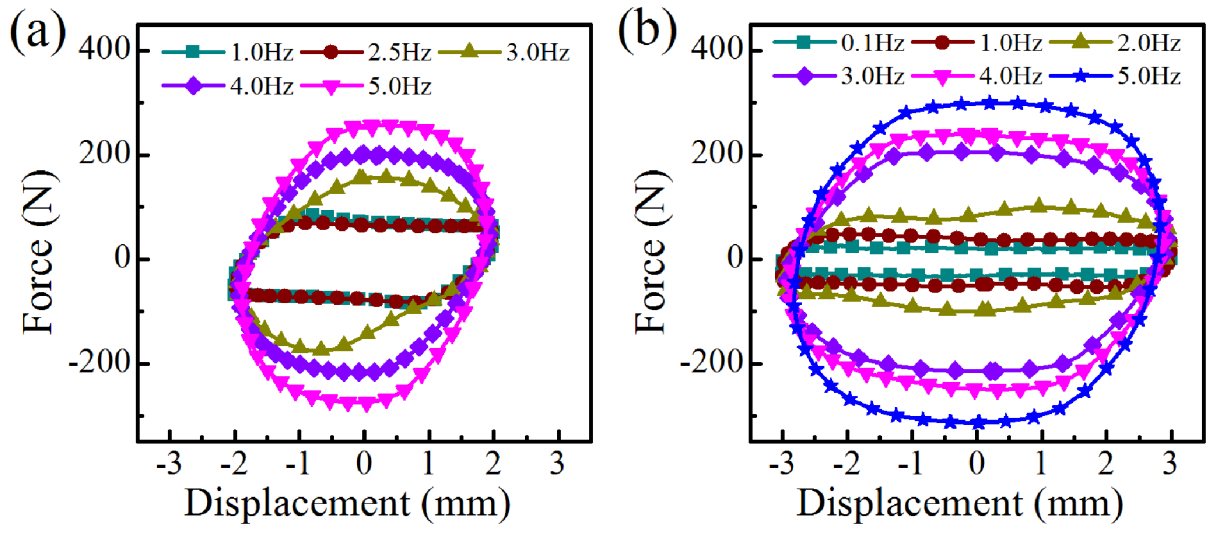

Figure 7. Force versus displacement at various frequencies and amplitudes of damper-2-65%STF: (a) A = 2 mm and (b) A = 3 mm.

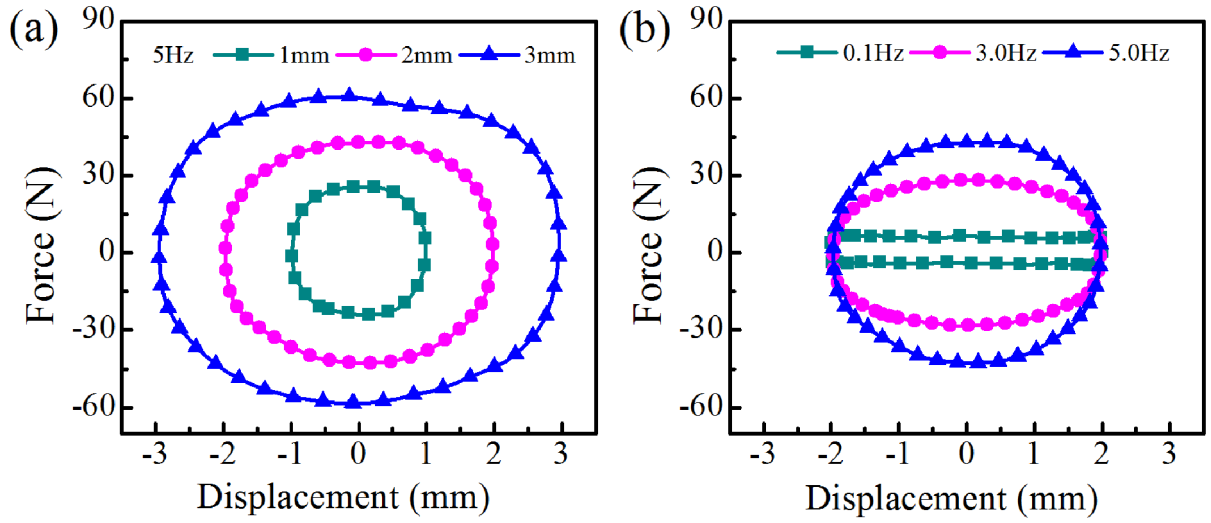

Figure 8. Force versus displacement at various frequencies and amplitudes of damper-2-SiOil: (a) f = 5 Hz and (b) A = 2 mm.

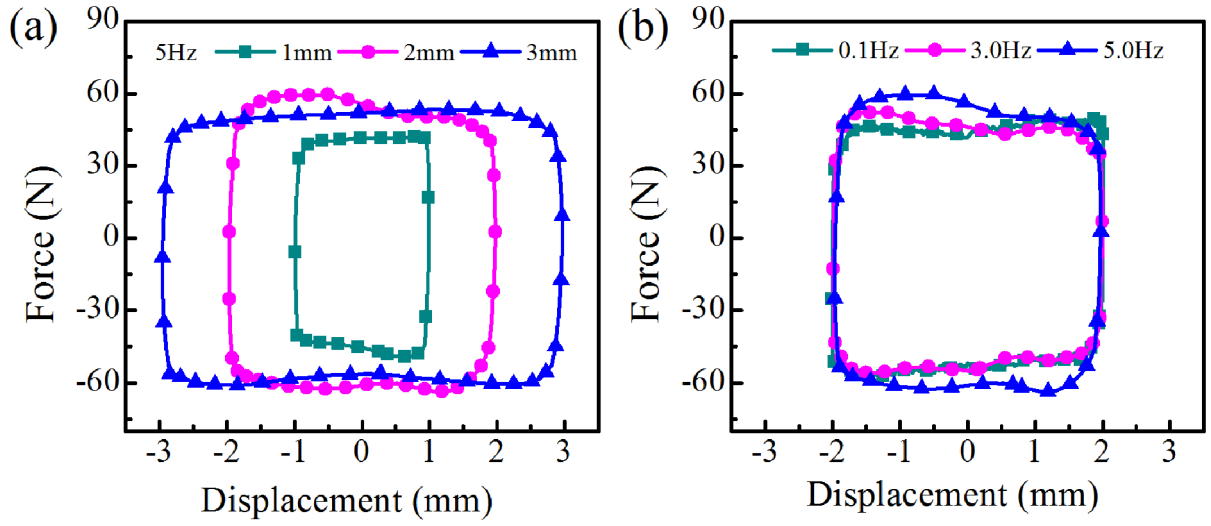

Figure 9. Force versus displacement at various frequencies and amplitudes of damper-2-60%STF: (a) f = 5 Hz and (b) A = 2 mm.

of force–displacement were rectangular (Figure 9). However, the loops of force–displacement of damper-2-SiOil were elliptic and no obvious incline in its major axis was found (Figure 8). Therefore, the damper-2-60%STF and damper-2-SiOil were worked on two different mechanisms. When the damper was pushing or drawing, a small amount of STF was driven into the seal groove and attached to the seal rings. It resulted in a considerable increase in friction force applied on the piston rod by seal rings. Thus, the friction force and viscous force dominated the output force of damper-2-60%STF and damper-2-SiOil, respectively. Because the maximum viscosity of 60 v/v% STF is smaller than that of Si-Oil sample, the viscous force resulting from the slight ST behavior should be lower in damper-2-60%STF. Similarly, the same results were observed in the damper-2-65%STF and damper-2-67%STF at low frequency and small amplitude, in which the ST behavior did not appear.

The dynamic properties of STF damper were sensitive to the frequency and amplitude; thus, the peak force as a function of peak velocity was investigated (Figure 10). For damper-2-67%STF with DST behavior, the curve of force–velocity can be divided into three states (see Figure 10(a)): the pre-shear-thickening state where the force is a small constant resulting from friction; the transition state where the force increases suddenly and the shear-thickened state where the force reaches a plateau value and increases slowly due to the viscoelasticity of STF. At the pre-shear-thickening state

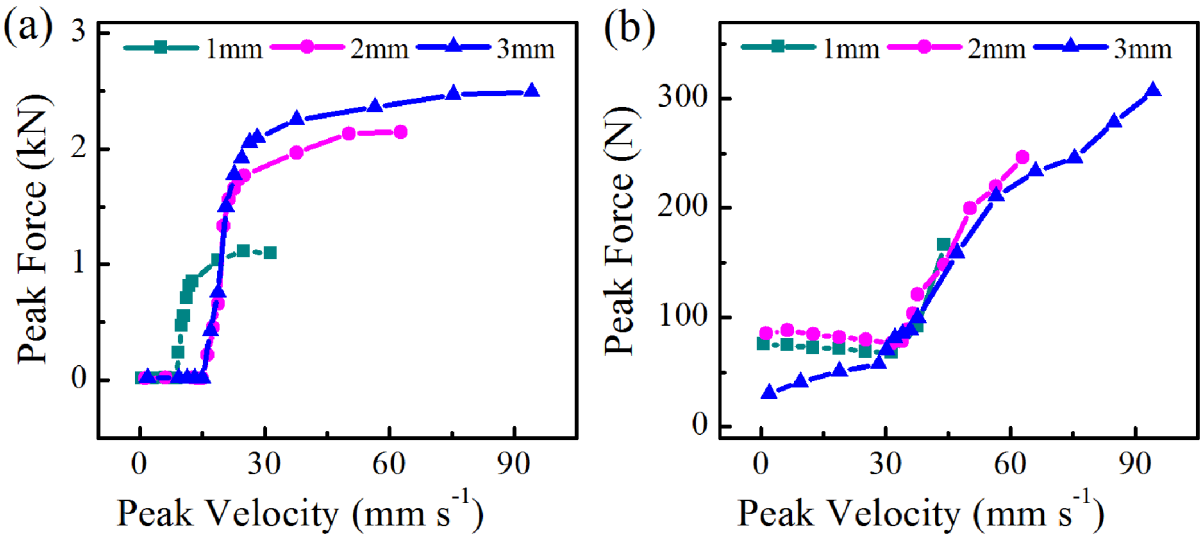

Figure 10. Peak force versus peak velocity at various amplitudes: (a) damper-2-67%STF and (b) damper-2-65%STF.

(with low piston velocity), the force generated from the friction between the piston rod and rubber seals was below 100 N. At the transition state (beyond critical velocity), the viscosity of STF increased sharply and a fluid–solid transition happened for a more densely packing suspension of 67 v/v% STF, which led to a sudden increase in the force of STF damper. At the shear-thickened state (with high piston velocity), a high-velocity stimulus was imposed and the STF showed a solid-like behavior. Thus, the viscoelastic force led to an increase in force with the amplitude. The effect of viscoelasticity generated from the solidification of STF contributed to the slowly increased force at high velocity. However, for damper-2-65%STF with CST behavior, the properties were different at high velocity (Figure 10(b)). The force increased continuously beyond critical velocity and the amplitudes performed nearly no influence on the force. Therefore, the viscous force dominated the output force of damper-2-65%STF.

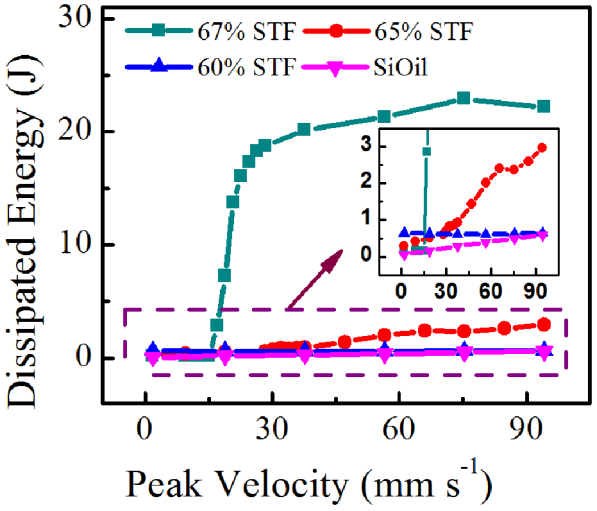

Figure 11. Dissipated energy per cycle versus peak velocity with different materials.

Energy dissipation. The energy dissipation capacity of STF damper was also studied in this work. Figure 11 shows the dissipated energy per cycle of different dampers as a function of peak velocity. Damper-2-SiOil showed a perfect Newtonian behavior and thus led to a linear increase in dissipated energy with the peak velocity. Similarly, three states could be obviously seen from the curve of damper-2-67%STF. The dissipated energy of damper-2-67%STF increased severely at transition state and reached a plateau which was much higher than the others at shear-thickened state. The dissipated energy of damper-2-65%STF increased continuously and its slope was larger than that of damper-2-SiOil, which showed the damper-2-65%STF performed a quasi-Newtonian behavior with a higher viscosity. The curve of damper-2-60%STF was a horizontal straight line because of the friction-dominated force. The tremendous difference demonstrates that the STF damper with more densely packing suspension has a greater ability of energy dissipation than the others, which can be utilized for devices of shock absorption or impact resistance.

Modeling of STF damper at shear-thickened state

Equivalent linear model. An equivalent linear model was used to depict the force–displacement characteristics of the STF damper. The model consists of an effective

stiffness term and an effective viscous damping term. The damper force can be expressed as (Zhang et al., 2008)

$$F = k_{eff}x + c_{eff}\dot{x} \tag{1}$$

where k_{eff} is the effective stiffness and c_{eff} is the effective viscous damping constant.

The effective stiffness is calculated from the experimental force–displacement curves of the STF damper and expressed as

$$k_{eff} = \frac{F^+ - F^-}{A^+ - A^-} \tag{2}$$

where F^+ and F^- are the forces at the displacements of A^+ and A^-. A^+ and A^- are the displacement at the end of compression and tension amplitudes of the piston from the original position, respectively. Therefore, k_{eff} is approximately the slope of the peak-to-peak value of the experimental hysteresis loop. However, the k_{eff} may not be accurate enough to characterize the damper before the transition because of the step change in the friction-dominated force at the ends of stroke.

The effective viscous damping constant is expressed as

$$c_{eff} = \frac{\varpi_d}{\pi\omega A^2} \tag{3}$$

where ϖ_d is the dissipated energy per cycle of the hysteresis loop and A is the amplitude for the displacement.

The curves of effective stiffness and damping constant versus peak velocity are shown in Figure 12. The tests were carried out on damper-2-67%STF at applied amplitude of 3 mm. The effective stiffness increased significantly at transition state. Then, it reached a plateau value of about 500 N mm^{-1} at shear-thickened state. The effective viscous damping constant also increased abruptly at a critical peak velocity, but it reached a maximum value of about 75 N s mm^{-1} at the beginning of shear-thickened state and decreased as the peak velocity increases. The significant increase in effective stiffness and effective viscous damping constant was ascribed to the severe shear thickening. With an increase in the peak velocity, the STF showed a solid-like behavior and became hard to flow. The viscoelasticity resulted in an intense nonlinear characteristic of damping force. Therefore, the viscoelastic force dominated in the output force of the STF damper. This explains why the force keeps a relative stable value at higher velocity. Hence, the effective stiffness reached a plateau value at shear-thickened state in terms of equation (2), in which the numerator as a difference between the positive and negative forces had no obvious change. Moreover, it is easy to understand the decrease in effective viscous damping constant at shear-thickened state. The effective viscous damping constant is the ratio of the dissipated energy and the product of angular frequency and the square of amplitude according to equation (3). No obvious increase in the dissipated energy was found at higher frequency and amplitude because of the stable output force so that the ratio decreases with an increase in the excited frequency at shear-thickened state.

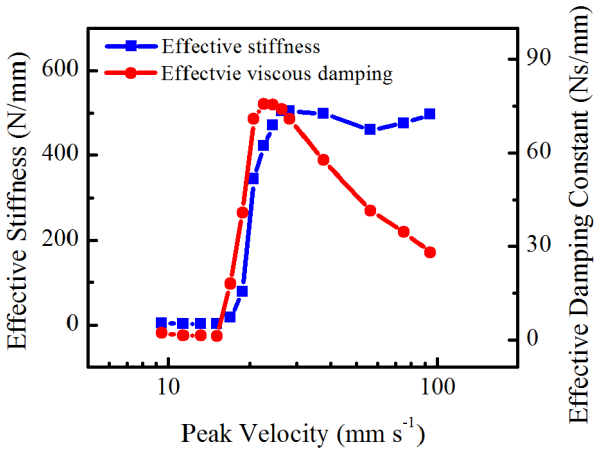

Figure 12. Effective stiffness and viscous damping constant versus peak velocity for damper-2-67%STF.

Equivalent nonlinear model. The characteristics of stiffness and viscous damping of STF damper can be generally given by the equivalent linear model shown in equation (1). However, the STF damper possessed obvious nonlinear characteristic at shear-thickened state. The linear model cannot accurately describe the STF damper's characteristics at shear-thickened state. A model that introduced power law to the equivalent linear model was employed to describe the output force of STF damper. The model is expressed as

$$F = kx + c|\dot{x}|^{\alpha} \cdot \mathrm{sgn}(\dot{x}) \tag{4}$$

where k is the stiffness, c is the viscous coefficient, sgn() is the sign function, and α is the power-law index, also known as velocity index.

The parameters were calculated by genetic algorithm according to the experimental data. The result showed that the parameters varied with different frequencies (Figures 13 and 14). In order to better describe the characteristics of STF damper, the relations between the parameters of equivalent model and frequency were fitted with two-order polynomial functions. The functions can be expressed as

$$k = a_1 + b_1 f + c_1 f^2 \tag{5a}$$

$$c = a_2 + b_2 f + c_2 f^2 \tag{5b}$$

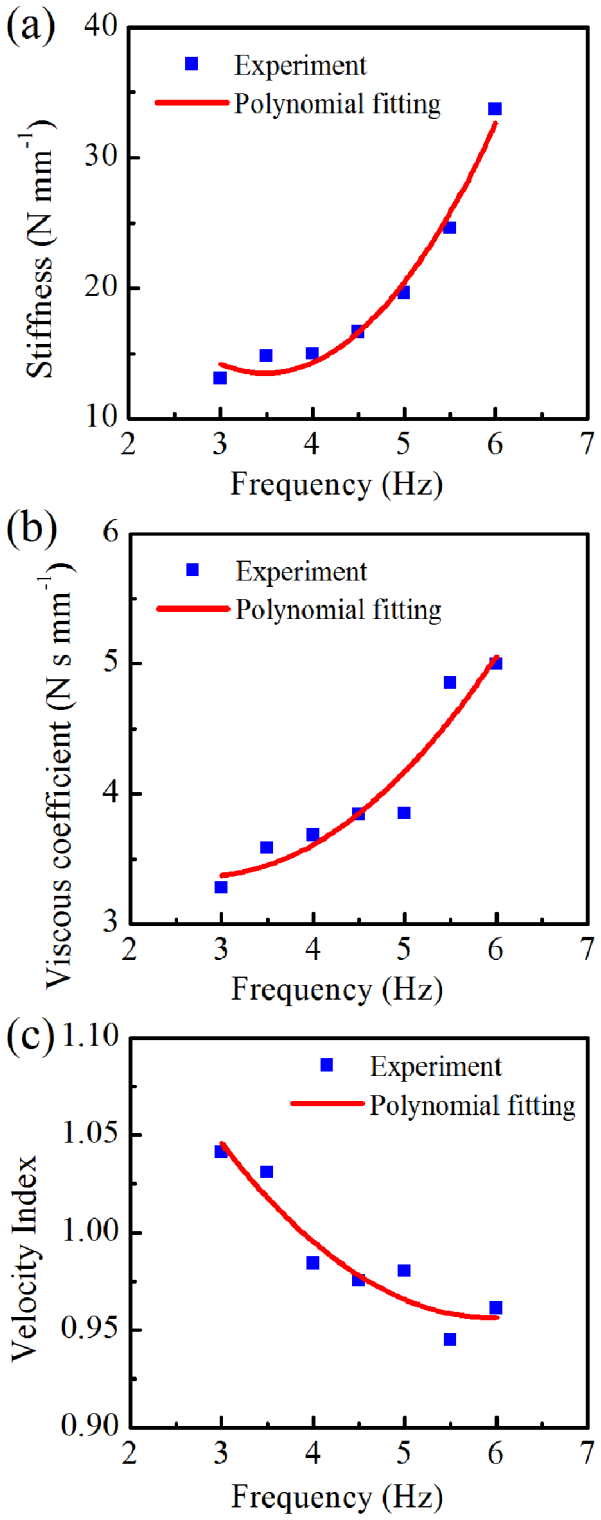

Figure 13. Polynomial fitting of parameters as a function of frequency for damper-2-65%STF: (a) stiffness, (b) viscous coefficient, and (c) velocity index.

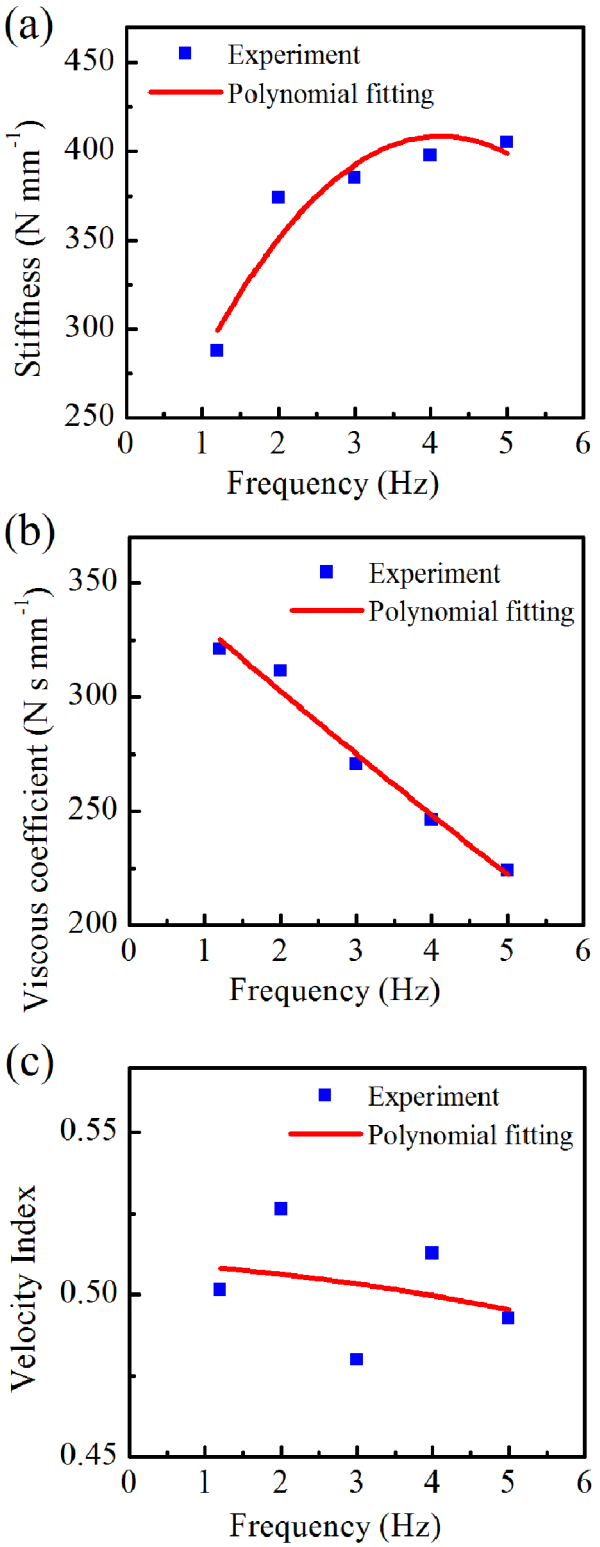

Figure 14. Polynomial fitting of parameters as a function of frequency for damper-2-67%STF: (a) stiffness, (b) viscous coefficient, and (c) velocity index.

$$\alpha = a_3 + b_3 f + c_3 f^2 \qquad (5c)$$

where a, b, and c are the fitting coefficients and f is the frequency.

The polynomial fitting curves and coefficients were determined by the least square fitting. The results are, respectively, shown in Figure 13, Figure 14, and Table

2. It can be seen that the stiffness and the viscous coefficient increased with the frequency for damper-2-65%STF, and the velocity index was around 1 and decreased with the frequency (Figure 13). It is similar to the equivalent linear model where the velocity index is fixed at 1 (equation (1)). The stiffness of damper-2-67%STF also increased with the frequency, but the viscous coefficient decreased and the velocity index was smaller than 1 (Figure 14). Because of the solidification of STF, the viscoelastic force dominates and dissipated energy cannot increase apparently as the velocity increases. Finally, the velocity index becomes smaller than 1 and the ratio of viscous force to total force decreases as the frequency increases. Therefore, the viscoelastic force dominates and the effect of viscous force is weakened at high frequency, which is similar to the experimental results.

Figure 15 shows the comparison between the experimental force and calculative force at various frequencies for damper-2-65%STF and damper-2-67%STF, respectively. The coefficients used in the calculation are listed in Table 2. It can be seen that this model agreed well with the experimental results. Thus, it is possible to characterize and predict the performance of STF damper at shear-thickened region via the equivalent nonlinear model.

Conclusion

In this work, a prototype STF damper was designed and developed. The maximum viscosity of the STF samples was tunable by adjusting particle volume fraction; thus, STF-based dampers with different mechanical properties can be constructed. The dynamic properties of these dampers were examined by MTS through a series of loading conditions. The hysteresis loops of force–displacement were obtained, and the effects of particle concentration and piston geometry on the damper were investigated. The experimental results showed that the particle concentration had a great influence on the STF damper's characteristics, in which the output force could be varied from 0.1 to 2.7 kN. With less densely packing STF of 60 v/v%, the ST behavior was slight and the damper force was kept constant at 60 N due to the friction between the seal rings and piston rod. With 65 v/v% STF, the damper force increased continuously to 0.3 kN and exhibited a quasi-Newtonian behavior with a higher viscosity. With more

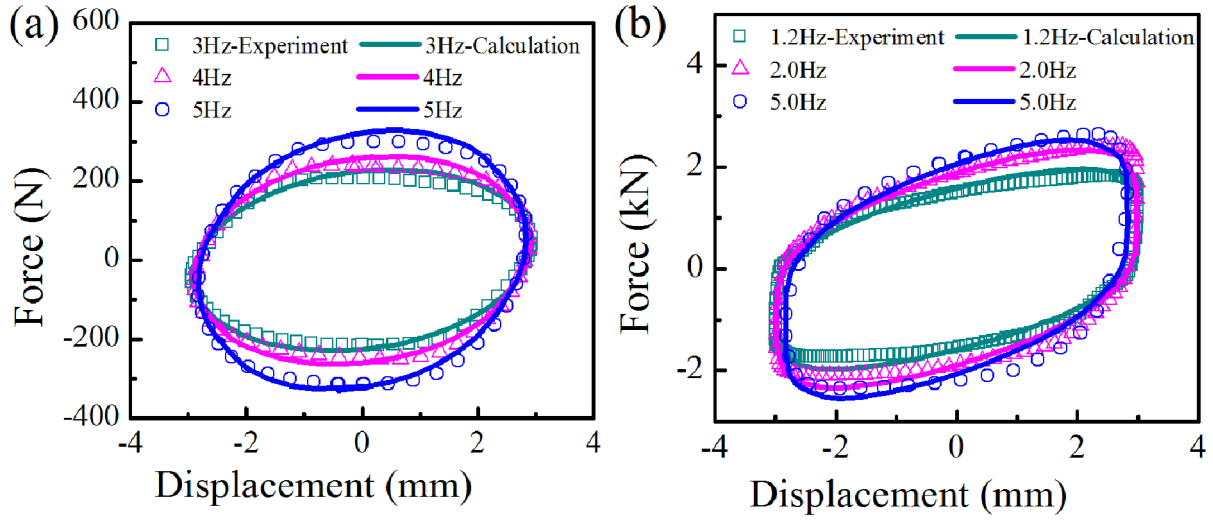

Figure 15. Comparison between experimental force and calculative force at various frequencies: (a) damper-2-65%STF and (b) damper-2-67%STF.

Table 2. The polynomial fitting coefficients for damper-2-65%STF and damper-2-67%STF.

Parameters	Damper-2-65%STF			Damper-2-67%STF		
	a	*b*	*c*	*a*	*b*	*c*
k	50.162	−21.070	3.0251	190.98	105.55	−12.793
c	4.600	−0.8938	0.1616	359.82	−29.295	0.3526
α	1.320	−0.1223	0.0103	0.5103	−0.00134	−3.26E−4

STF: shear thickening fluid.

densely packing STF of 67 v/v%, the damper force was raised to 2.7 kN and a nonlinear viscoelastic behavior was obtained due to the solidification of STF. Moreover, the annular gap had a greater influence on the output force than the piston length. The damper with smaller annular gap and longer piston provided larger output force and lower critical frequency. The dissipated energy per cycle of damper with more densely packing STF was much higher than the other dampers, which implied a great ability for devices of shock absorption or impact resistance. A model composed of an equivalent stiffness term and a power-law viscous damping term was employed to characterize the nonlinear behavior of STF damper at shear-thickened state. The parameters in the equivalent nonlinear model were investigated as a function of excitation frequency. The calculative damper force agreed well with the experimental results, which demonstrated a possibility for predicting the performance of STF damper at shear-thickened state.

Declaration of Conflicting Interests

The authors declared no potential conflicts of interest with respect to the research, authorship, and/or publication of this article.

Funding

The author(s) disclosed receipt of the following financial support for the research, authorship, and/or publication of this article: Financial supports from the National Natural Science Foundation of China (Grant Nos 11372301, 11125210, 11102202) and the National Basic Research Program of China (973 Program, Grant No. 2012CB937500) are gratefully acknowledged.

References

Barnes HA (1989) Shear-thickening (dilatancy) in suspensions of nonaggregating solid particles dispersed in Newtonian liquids. *Journal of Rheology* 33(2): 329–366.

Bender J and Wagner NJ (1996) Reversible shear thickening in monodisperse and bidisperse colloidal dispersions. *Journal of Rheology* 40(5): 899–916.

Bica I, Liu YD and Choi HJ (2013) Physical characteristics of magnetorheological suspensions and their applications. *Journal of Industrial and Engineering Chemistry* 19(2): 394–406.

Boersma WH, Laven J and Stein HN (1995) Computer-simulations of shear thickening of concentrated dispersions. *Journal of Rheology* 39(5): 841–860.

Brown E and Jaeger HM (2014) Shear thickening in concentrated suspensions: phenomenology, mechanisms and relations to jamming. *Reports on Progress in Physics* 77(4): 046602.

Brown E, Forman NA, Orellana CS, et al. (2010) Generality of shear thickening in dense suspensions. *Nature Materials* 9(3): 220–224.

Cheng X, McCoy JH, Israelachvili JN, et al. (2011) Imaging the microscopic structure of shear thinning and thickening colloidal suspensions. *Science* 333(6047): 1276–1279.

Dawson MA, McKinley GH and Gibson LJ (2009) The dynamic compressive response of an open-cell foam impregnated with a non-Newtonian fluid. *Journal of Applied Mechanics—Transactions of the ASME* 76(6): 061011.

Dyke SJ, Spencer BF, Sain MK, et al. (1996) Modeling and control of magnetorheological dampers for seismic response reduction. *Smart Materials and Structures* 5(5): 565–575.

Fall A, Bertrand F, Ovarlez G, et al. (2012) Shear thickening of cornstarch suspensions. *Journal of Rheology* 56(3): 575–591.

Fischer C, Bennani A, Michaud V, et al. (2010) Structural damping of model sandwich structures using tailored shear thickening fluid compositions. *Smart Materials and Structures* 19(3): 035017.

Foss DR and Brady JF (2000) Structure, diffusion and rheology of Brownian suspensions by Stokesian Dynamics simulation. *Journal of Fluid Mechanics* 407: 167–200.

Helber R, Doncker F and Bung R (1990) Vibration attenuation by passive stiffness switching mounts. *Journal of Sound and Vibration* 138(1): 47–57.

Hoffman RL (1998) Explanations for the cause of shear thickening in concentrated colloidal suspensions. *Journal of Rheology* 42(1): 111–123.

Iyer SS, Vedad-Ghavami R, Lee H, et al. (2013) Nonlinear damping for vibration isolation of microsystems using shear thickening fluid. *Applied Physics Letters* 102(25): 251902.

Jiang WQ, Sun YQ, Xu YL, et al. (2010) Shear-thickening behavior of polymethylmethacrylate particles suspensions in glycerine-water mixtures. *Rheologica Acta* 49(11–12): 1157–1163.

Jolly MR, Bender JW and Carlson JD (1999) Properties and applications of commercial magnetorheological fluids. *Journal of Intelligent Material Systems and Structures* 10(1): 5–13.

Kim JW, Cho YH, Choi HJ, et al. (2002) Electrorheological semi-active damper: polyaniline based ER system. *Journal of Intelligent Material Systems and Structures* 13(7–8): 509–513.

Laun HM, Bung R and Schmidt F (1991) Rheology of extremely shear thickening polymer dispersions (passively viscosity switching fluids). *Journal of Rheology* 35(6): 999–1034.

Lee HS and Choi SB (2000) Control and response characteristics of a magneto-rheological fluid damper for passenger vehicles. *Journal of Intelligent Material Systems and Structures* 11(1): 80–87.

Lee YS and Wagner NJ (2006) Rheological properties and small-angle neutron scattering of a shear thickening, nanoparticle dispersion at high shear rates. *Industrial & Engineering Chemistry Research* 45(21): 7015–7024.

Lee YS, Wetzel ED and Wagner NJ (2003) The ballistic impact characteristics of Kevlar (R) woven fabrics impregnated with a colloidal shear thickening fluid. *Journal of Materials Science* 38(13): 2825–2833.

Li WH and Du H (2003) Design and experimental evaluation of a magnetorheological brake. *International Journal of Advanced Manufacturing Technology* 21(7): 508–515.

Maranzano BJ and Wagner NJ (2001) The effects of interparticle interactions and particle size on reversible shear thickening: hard-sphere colloidal dispersions. *Journal of Rheology* 45(5): 1205–1222.

Maranzano BJ and Wagner NJ (2002) Flow-small angle neutron scattering measurements of colloidal dispersion microstructure evolution through the shear thickening transition. *Journal of Chemical Physics* 117(22): 10291–10302.

Srivastava A, Majumdar A and Butola BS (2012) Improving the impact resistance of textile structures by using shear thickening fluids: a review. *Critical Reviews in Solid State and Materials Sciences* 37(2): 115–129.

Wereley NM, Pang L and Kamath GM (1998) Idealized hysteresis modeling of electrorheological and magnetorheological dampers. *Journal of Intelligent Material Systems and Structures* 9(8): 642–649.

Ye F, Zhu W, Jiang WQ, et al. (2013) Influence of surfactants on shear-thickening behavior in concentrated polymer dispersions. *Journal of Nanoparticle Research* 15(12): 2122.

Zhang XZ, Li WH and Gong XL (2008) The rheology of shear thickening fluid (STF) and the dynamic performance of an STF-filled damper. *Smart Materials and Structures* 17(3): 035027.

Zong LH, Gong XL, Xuan SH, et al. (2013) Semi-active H infinity control of high-speed railway vehicle suspension with magnetorheological dampers. *Vehicle System Dynamics* 51(5): 600–626.